### Title

Voltage-Gated Closed-Loop Control of Small-Molecule Release from Alumina-Coated Nanoporous Gold Thin Film Electrodes




### Journal

Advanced Functional Materials, 28(29)

### ISSN

1616-301X



### Authors

Li, Zidong
Polat, Ozge
Seker, Erkin



### Publication Date

2018-07-01

### DOI

10.1002/adfm.201801292

Peer reviewed

DOI: 10.1002/adfm.201801292
**Article type: Full Paper**

# Voltage-Gated Closed-Loop Control of Small-Molecule Release from Alumina-Coated Nanoporous Gold Thin Film Electrodes

*Zidong Li[1], Ozge Polat[2], and Erkin Seker[3,*]*

Zidong Li
Department of Biomedical Engineering – University of California, Davis
Davis, CA 95616, USA

Dr. Ozge Polat
Department of Chemical Engineering – University of California, Davis
Davis, CA 95616, USA

Prof. Erkin Seker
Department of Electrical and Computer Engineering – University of California, Davis
Davis, CA 95616, USA
Email: eseker@ucdavis.edu

**Keywords:** drug delivery, iontophoresis, closed-loop control, nanoporous gold, microfluidics

Precise timing and dosing of potent small-molecule drugs carries significant potential for effective pharmaceutical management of disorders that exhibit time-varying therapeutic windows such as epilepsy. This study demonstrates the use of alumina-coated nanoporous gold (np-Au) thin film electrodes for iontophoretic release of fluorescein as a small-molecule drug surrogate with picogram dosing and a few seconds temporal resolution. A custom microfluidic platform was engineered to trigger molecular release from an integrated np-Au chip and monitor the resulting time-varying fluorescein concentration. Following a systematic study of the influence of applied voltage on loading capacity and release kinetics, a LabVIEW-based closed-loop control interface was employed to demonstrate voltage-gated fluorescein release with pre-programmed arbitrary concentrations waveforms.

## 1. Introduction

Timing and dose of therapeutic administration is critical for successful management of disorders and study of basic biological phenomena influenced by soluble factor signals. While pharmaceutical administration in bolus form is still common, advances in time-released drugs is already improving therapeutic outcomes for numerous diseases such as glaucoma,[1] Parkinson's disease,[2] and inflammatory bowel disease.[3] For all pharmaceutical-based treatment, an important figure of merit is to keep the available drug amount in the body within a therapeutic window; where below the lower limit, the drug is not effective and above the upper limit, the drug is toxic. This becomes especially important for potent drugs (e.g., digoxin,[4] phenytoin,[5] and lithium[6]), where the therapeutic window is very narrow. For such drugs, there is continuous monitoring of possible side effects and symptomatic benefits. In tandem, several drug delivery technologies focused on controlling the release with the goal of keeping the available drug dose within the therapeutic window. These include macro-scale infusion pumps[7] and miniaturized microelectromechanical systems (MEMS)-based pumps that are under development.[8] For both technologies, the pharmaceuticals are typically delivered within a vehicle solution (typically saline), which may increase the local pressure at the delivery area if it is delivered into tissue rather than blood. On the other hand, delivery of therapeutics directly into the tissue has significant advantages for some cases, such as blood-brain-barrier reducing therapeutic efficiency if the delivery route is via blood.[9] In order to take advantage of direct delivery into tissue but reduce the volume injected, more potent drugs or higher concentrations can be injected into the tissue. This naturally requires tighter control of the delivered dose. In addition, the need for a vehicle solution and associated complications can be completely circumvented by directly delivering the pharmaceuticals. In part to address these challenges, molecular release platforms have been developed, where drug molecules are delivered via release from non-degrading porous materials[10] or via dissolution from degrading polymeric materials.[11] In these systems, the influence of decreasing concentration

gradient, which reduces the drug release rate hence the released amount over time, was mitigated by employing zero-order (concentration-independent) release from pores with comparable size to the hydrodynamic radius of drug molecules and by controlling the dissolution rate of the polymeric carriers. While these technologies under development have shown significant promise, there is an added challenge for some cases, where the therapeutic window is time-varying, that is, at any given time the necessary dose changes. For example, in a transient disorder like epilepsy, a seizure needs to be suppressed either pharmaceutically or electrically as there is need, and the on-demand intervention should be ceased when there is no symptom. While there have been promising advances for the latter (electrical) approach[12] and only a handful demonstrations of triggered molecular release,[13] the ability to delivery molecules on demand at arbitrary doses is at its infancy.

Taken together, desirable features for the next generation pharmaceutical delivery platforms require the ability to (i) deliver molecules without infusing large carrier volumes, (ii) administer arbitrary doses, (iii) hold small form factor; and (iv) be scalable and amenable to multiplexing. In this paper, we employ nanoporous gold (np-Au) as a novel material to address these challenges. Np-Au is produced by dissolving silver from a silver-rich gold alloy in heated nitric acid, where gold atoms go under surface diffusion to create a bicontinuous open-pore structure.[14] A wide range of attractive features, including high surface area-to-volume ratio,[15] tunable morphology[16] and surface chemistry,[17] biocompatibility,[18] electrical conductivity,[16a] and compatibility with conventional microfabrication techniques,[19] have led to interest from the sensing and catalysis community. These features, also desirable for precise control of molecular release, enable high small-molecule loading capacity and release kinetics, paved the way for np-Au's use in molecular release applications.[20] Here, we report on alumina-coated np-Au thin films integrated into a

microfluidic test platform for achieving closed-loop control of small-molecule release with arbitrary time-varying waveforms.

## 2. Results and Discussion

### 2.1. Rationale for Using Alumina-Coated Np-Au Films

The np-Au thin films were 450 nm-thick and exhibited a homogenous porosity with an average pore size of 50 nm. When the np-Au thin films were loaded with fluorescein (a small-molecule drug surrogate[21]), this geometry yielded a loading capacity of 0.75 μg/cm$^2$ (mass per unit footprint of np-Au thin film pattern). The primary mechanism of loading is non-specific adsorption of fluorescein onto np-Au ligaments via van der Waals interactions.[17a] The challenge is that when np-Au is immersed in a physiologically-relevant solution, like phosphate-buffered saline (PBS), the high affinity of halide ions to gold results in replacement of surface-adsorbed fluorescein and burst release.[20a, 22] We have previously mitigated this problem by immobilizing 6-mercapto-1-hexanol onto the np-Au, which effectively reduced the direct interaction of halide with gold.[17a] However, hydroxyl groups, also reduced the loading capacity of fluorescein, plausibly due to hydroxyl groups being less polarizable compared to the gold atoms, thereby leading to a reduced van der Waals interaction. A strategy to overcome the reduced loading capacity while still preventing the halide sensitivity might be to leverage the electrical conductivity of hexanol-decorated np-Au is to apply a positive electric voltage with respect to a counter/reference electrode. This, in turn, would electrostatically attract the fluorescein molecules to the surface. Unfortunately, self-assembled monolayers (SAMs) are not entirely impermeable to small ions and charge carries and suffer from poor dielectric break-down voltages. This, in turn, results in applied voltages leading to undesirable faradaic electrochemical reactions that are responsible for producing undesirable reactive species (**Figure 1**). The faradaic peaks observed at 0.25 V, -0.01 V, 0.19 V and –0.06

V with respect to a Ag/AgCl reference electrode, both visible for bare gold and hexanol-coated gold, are due to gold oxidation/reduction, as reported by us and others.[21, 23] Finally, in order to resolve both the halide-sensitivity and faradaic reactions problem, we chose a solid dielectric material, aluminum oxide (alumina) deposited with the atomic layer deposition technique. Alumina deposition leads to conformal coating of high aspect-ratio np-Au thin films[24] and remains biocompatible in neural cell cultures.[18a] The alumina layer is approximately 2.5 nm-thick based on the deposition recipe and corresponding growth rate described by Biener et al.[24]. The cyclic voltammogram of alumina-coated np-Au indeed revealed no faradic peaks, suggesting a pinhole-free surface coverage (Figure 1).

To verify if alumina is sensitive to halide ions, we incubated alumina-coated and uncoated np-Au in 10 mM fluorescein solution prepared in deionized (DI) water for 16 hours under open-circuit voltage. The fluorescein-loaded alumina-coated and uncoated np-Au were then immersed in DI water and phosphate buffered saline (PBS) solution separately to monitor the release kinetics. As shown in **Figure 2**, compared to DI water, PBS significantly increased both the loading capacity and release kinetics of uncoated np-Au. While for alumina-coated np-Au, the release in both PBS and DI water were negligible, which demonstrated that the alumina layer insensitive to halide and functioned successfully to prevent the uncontrollable burst release. Alumina (isoelectric point of 8.6) acquires a slightly positive surface charge in PBS (pH of 7.2),[25] while fluorescein molecules are negatively charged due to its isoelectric point lower than pH of PBS (~7,4).[26] The loading capacity for alumina-coated np-Au was expected to have increased due to the electrostatic interactions between fluorescein molecules and the alumina surface. However, the loading capacity was surprisingly minimal for the alumina-coated np-Au when loaded under open-circuit voltage. We attribute the hydroxyl moieties formed on the alumina surface that resemble to the hexanol-modified surface described above. Taken together, the alumina coating reduced both chloride and fluorescein

interactions with the surface.

An advantage of alumina is that it is a dielectric material that can be easily polarized under an applied voltage displaying a negatively- or positively-charged surface, mimicking an electrolytic capacitor in charged state.[27] Therefore, a positive voltage on the alumina-coated np-Au film should attract fluorescein molecules (*loading state*) while the application of a negative voltage should repel the loaded fluorescein molecules (*release state*). In turn, this should allow voltage-gated iontophoretic release of fluorescein molecules from the np-Au thin film. It should be noted that for the rest of paper, alumina-coated np-Au is used in all voltage-gated release experiment.

### 2.2. Voltage-Gated Iontophoretic Release Platform

An iontophoretic release study platform was engineered in order to establish a robust electrical connection to the np-Au electrode and monitor molecular release from np-Au in real-time. The platform has three main components (**Figure 3A**): (i) a 3D printed microfluidic chip holder made in polylactic acid (PLA); (ii) a microfluidic device used for electrically-controlled release experiment; and (iii) a laser-cut printed circuit board (PCB) for the electrical connection. The alumina-coated np-Au electrode was mounted at the base of the microfluidic device, where the released fluorescein molecules are carried with the infused liquid past below the microscope objective for acquiring the fluorescence intensity. A spring-loaded copper pin soldered at the tip of the PCB arm contacted the alumina-coated np-Au electrode surface through a via in the microfluidic device. The slight pressure exerted by the copper pin is enough to break the alumina coating and establishing electrical connectivity. An additional via was created to make a secondary contact to the alumina-coated np-Au electrode for verifying electrical connectivity. The ability to vary the contact pressure between the pin and the electrode allowed for achieving a robust electrical connection (**Figure S2**). A microfluidic chip holder was designed to mechanically support the np-Au electrode opposing

the force exerted by the pin, thereby preventing possible leakage.

Initially, a three-electrode configuration was used to have precise control of the applied voltage on the np-Au electrode. The alumina-coated np-Au electrode served as the working electrode and the voltage was applied through the PCB arm. A flow-through Ag/AgCl reference electrode was connected to the outlet of the microfluidic device, and a platinum wire counter electrode was immersed inside the glass reservoir filled with PBS (Figure 3B). This integrated setup allowed for both microfluidic control (flow rate) and electrical control (iontophoretic release).

### 2.3. Influence of Applied Voltage on Molecular Loading

As mentioned earlier, the loading capacity of alumina-coated np-Au under open-circuit voltage is negligible (Figure 2); therefore, it is necessary to stabilize surface-molecule interactions, where the electrical conductivity of np-Au gives the opportunity to impose electrostatic interactions. In order to establish the loading capacity and release kinetics, we applied a positive voltage on the np-Au electrode while it is immersed in concentrated fluorescein solution. The inward concentration gradient, coupled with the iontophoretic movement of fluorescein due to the applied voltage, resulted in loading of np-Au with fluorescein. In order to study the subsequent release profile, a small negative voltage (-0.5 V) was applied to accelerate the release. Following the completion of the release (judged by steady-state release profile, **Figure 4**), the same alumina-coated np-Au chip was loaded following the same protocol yet at different voltages (i.e., +0.2 V, +0.4 V and +0.9 V with respect to Ag/AgCl). The cumulative release profile reached a higher steady-state value (representative of the loading capacity) for samples loaded at a higher voltage (Figure 4). This is not surprising, since a larger number of molecules are expected to migrate into np-Au, as the applied electric field overcomes the outward concentration gradient as more molecules are loaded. In addition, by sustaining the applied voltage during the rinsing step ensured that the

loaded species were not washed away, which is an important capability to prevent passive drug release in a biological implant. The loading capacity was directly proportional to the applied loading voltage. Surprisingly, the corresponding half-life (duration to release 50% of the loaded fluorescein) was inversely proportional to the applied loading voltage (Figure 4 inset), that is, a larger number of loaded molecules resulted in a faster release (**Figure S4**).

It is worthwhile elaborating on the release mechanisms, as it differs from the release from np-Au that is loaded via purely concentration gradient-driven influx of fluorescein without any applied voltage. For the open-circuit voltage loading, the resulting loading capacity was 1.12 $\mu g/cm^2$. We have reported that majority of the loading capacity for bare np-Au is due to surface-adsorption of fluorescein molecules as opposed to volumetric containment of fluorescein solution within the pores.[17a, 21] Based on this notion, the loading capacity is largely due to a monolayer of fluorescein molecules physio-adsorbed with a packing density of 10 molecules/$nm^2$ assuming hexagonal packing and a fluorescein hydrodynamic radius of 0.58 nm (calculated by Stokes−Einstein equation).[21] For a similar np-Au sample but with 2.5 nm-thick alumina coating, the surface area enhancement factor (surface area with respect to that for a planar gold electrode) reduced slightly from 18.9 to 17.9. Despite this, the loading capacity for alumina-coated np-Au (loaded under a positive voltage) yielded much higher loading capacities. Specifically, for 0.2 V, 0.4 V, and 0.9 V, the resulting loading capacities were 2.11 $\mu g/cm^2$, 2.95 $\mu g/cm^2$, 4.56 $\mu g/cm^2$ respectively, compared to 1.12 $\mu g/cm^2$ for bare np-Au. This suggests that the applied voltage results in multi-layer packing of fluorescein over the np-Au surfaces. It is probable that the multi-layer packing of negatively-charged fluorescein molecules is responsible for the reduced half-life for higher loading capacities (**Figure S3**). For fluorescein loading under applied positive voltage, negatively-charged fluorescein molecules are attracted to the surface and electrically screen the induced surface charge on the alumina shell (**Figure 5A**). With higher applied voltages, more fluorescein

molecules are attracted to the surface to conserve the charge balance, leading to a thicker multi-layer stacking (Figure 5B). This process of increasing the fluorescein concentration at the surface stores energy both through entropic means (organizing molecules in small volume) and through electrostatic means (keeping negatively-charged molecules in close proximity). When the applied voltage is removed, the electrostatic repulsion accelerates the fluorescein dispersion (Figure 5D), likely increasing the mobility of the particles compared to the dispersion of neutral particles (which is driven by random Brownian motion, that is, diffusion) (Figure 5C). This putative mechanism is likely the reason for the observed inverse proportionality between release half-life and applied loading voltage.

### 2.4. Influence of Applied Voltage on Release Kinetics

Following the influence of applied voltage on small-molecule loading, we studied its influence on molecular release from np-Au. The alumina-coated np-Au loaded with fluorescein for one hour under +1 V, was pulsed with different negative voltages (i.e., open-circuit, -0.1 V, -0.2 V, -0.4 V and -0.6 V each with a 30 s-duration). In between each pulse, +1 V was applied to halt passive (concentration gradient-driven) fluorescein release. The same triggered-release protocol was performed for two additional cycles without reloading the np-Au samples with fluorescein (**Figure 6**). The first immediate observation is that with increasing magnitude of the negative applied voltage, the fluorescein release rate increases within each cycle. In order to quantify this observation, we calculated the relative amount of fluorescein released during each pulse with respect to the total amount of fluorescein released during each cycle, as illustrated with individual data points for the corresponding cycle (Figure 6 inset). Furthermore, we determined the *average release rate* by dividing the cumulative amount for each voltage in each cycle by the applied voltage duration (Figure 6 blue dashes). When the *relative released amount* (percentage release) per each applied voltage is averaged across the different cycles (indicated with columns in Figure 6 inset), it is seen

that the percent release is independent of the amount of fluorescein present within the np-Au electrode at any given time. While this is an interesting result, in practice it is necessary to control the *absolute released amount* (e.g., delivered drug dose). It is clear that the same applied voltages lead to very different release rates (consequently absolute release amounts) as the fluorescein depot in np-Au is depleted. This highlights the need for a closed-loop control, where the applied voltage can be varied to maintain a specific released dose setpoint, which will be discussed next.

### 2.5. Closed-Loop Control of Molecular Release

In the studies described until now, a three-electrode configuration was used to have precise control of the applied voltage on the np-Au electrode to fully characterize the system. In order to reduce the complexity of the platform and simplify the electronic control circuitry, we switched to a two-electrode configuration for performing the closed-loop controlled release. In order to maintain defined molecular release profiles, a LabVIEW interface was created to continuously monitor time-varying fluorescence intensity due to released fluorescein traveling down the microfluidic channel (**Figure 7**). Briefly, in this control system, based on the difference (error) between actual released amount (measured signal) and intended release (setpoint), a proportional-integral-derivative (PID) module in LabVIEW determines the electrical voltage (control signal) to reduce the error signal (**Figure S4, S5,** and **S6**). Specifically, the controller prescribed a positive voltage to suppress the molecular release if the actual released amount overshot above the setpoint. Conversely, the controller prescribed a negative voltage to increase the released amount if the actual released amount undershot the setpoint. This control scheme allows for molecular release profiles in any arbitrary shape.

In order to challenge the closed-loop control system, we picked a complex non-monotonous staircase waveform as the time-varying setpoint. The instantaneous release profile (non-cumulative amount) of fluorescein molecules under closed-loop control is shown in **Figure 8**,

where the measured fluorescence intensity (blue line; surrogate for released fluorescein amount) is overlaid on the setpoint waveform (red line). The orange line indicates the computed control signal (applied voltage) to release fluorescein with adherence to the setpoint waveform. Due to the high initial fluorescein depot in np-Au (hence the larger concentration gradient for fluorescein outflux), the control is less accurate and the fluorescein release is more erratic. This is also in part due to the time delay (2.6 s) between the fluorescein release location (np-Au) and the downstream fluorescein observation region (microscope objective), which can be mitigated by a different design.

In order to assess the responsiveness of np-Au electrode in triggering molecular release due to the applied voltage signal, we conducted a cross-correlation analysis between the measured fluorescence intensity (blue line) and the applied voltage (orange line), focusing on the initial 28.2 second segment (**Figure S7**). We introduced a 2.6 s offset ($\Delta t$) to the data to compensate for the convective transport duration between the np-Au surface and the observation region underneath the microscope objective. The cross-correlation coefficient was as high as 0.6, indicating that the on-demand release of fluorescein follows the fine voltage spikes. The lack of a perfect correlation may be due to the different features in the fluorescence intensity and applied voltage waveforms. It is striking that fluorescence intensity (triggered fluorescein release) follows the applied voltage fluctuations with a periodicity of approximately two seconds (Figure S7). This is an important observation that suggests that given an effective control system is used with advanced control algorithms,[28] in principal molecular release with high temporal resolution can be achieved.

### 3. Conclusion

We have demonstrated a closed-loop controlled platform that achieves real-time monitoring of molecular release under applied voltages. The conformal anodic alumina coating on np-Au

electrode mitigated sensitivity to halides in physiological buffer and allowed for applying higher loading voltage without producing undesirable faradaic reactions. The higher loading voltages exhibited a higher loading capacity and consequently a faster release kinetics due to electrostatic repulsion between tightly-packed negatively-charged fluorescein molecules. By interfacing this voltage-gated molecular release platform to LabVIEW platform, we have achieved molecular release in an arbitrary time-varying concentration profiles with dosing as low as below 120 pg/min. In addition, a cross-correlation analysis of the fluorescein release in response to applied voltage fluctuations revealed that the voltage-gated molecular release can be achieved with a high spatial resolution. The microfabrication-compatibility of np-Au should allow for creating multiple electrodes for the delivering different drug molecules at arbitrary locations and waveforms. In addition, an array of drug-delivery electrodes can be activated in different group sizes to attain delivery of very small or large doses, exhibiting unparalleled dynamic range of dosing. Future work focuses on methods to replenish drug depot and *in situ* monitoring of molecular release (e.g., via electrochemical means) for an integrated closed-loop control in small form factor. Taken together, we expect the platform to create new opportunities for multifunctional biointerfaces (e.g., neural electrodes) that can deliver soluble factors (e.g., neuromodulators) at physiologically-relevant time scales and doses.[29]

## 4. Experimental Section

*Materials and instrumentation*: Sulfuric acid (96%) and hydrogen peroxide (30%) were purchased from J. T. Baker. Nitric acid (70%) and fluorescein sodium were obtained from Sigma-Aldrich. Thin glass coverslips (0.15 mm-thick) and glass slides (1 mm-thick) were obtained from Electron Microscopy Sciences. Epoxy adhesive was obtained from DEVCON. Polydimethylsiloxane (PDMS) was purchased from Dow Corning. Gold, silver, and chrome targets (99.95% pure) were obtained from Kurt J. Lesker. PalmSens potentiostat was used for

the three-electrode configuration to study how voltage influences the loading capacity and release kinetics. A data acquisition instrument (National Instrument USB-6001) and Basler acA1920-40um USB 3.0 camera were interfaced with LabVIEW to apply voltage (in two-electrode configuration) and capture the real-time release during the closed-loop controlled release experiment.

*Fabrication of standard np-Au films and alumina-coated np-Au films*: Np-Au films were patterned on piranha-cleaned (1:4 volume ratio of hydrogen peroxide and sulfuric acid) coverslips by sequentially sputter-depositing a 160 nm-thick chrome adhesive layer, an 80 nm-thick gold seed layer, and a 600 nm-thick silver-gold alloy layer. After deposition, the samples were dealloyed by immersion in heated (55°C) undiluted nitric acid to produce the np-Au films. The dealloyed chips were rinsed with copious amounts of DI water. The alumina-coated np-Au films were produced by coating standard np-Au films with conformal, 2.5 nm-thick aluminum oxide (alumina) by atomic layer deposition.

*Fluorescein loading and releasing under open-circuit voltage*: The alumina-coated and uncoated np-Au chips were placed in individual 0.2 mL centrifuge tubes filled with 10 mM fluorescein solution prepared in deionized (DI) water at room temperature for 16 hours. The loaded alumina-coated and bare np-Au chips were rinsed in DI water to remove the residual fluorescein molecules from the glass coverslip and dried under nitrogen gas flow. The fluorescein-loaded chip was mounted onto the microfluidic platform over the bottom fluid access window at the microfluidic channel floor to disperse the released molecules into the elution medium inside the channel. The elution medium was introduced from the inlet glass reservoir filled with DI water or PBS to the outlet connected to a syringe pump that withdrew at 1 μL/min volumetric rate.

*Fluorescein loading and release under applied voltage*: The alumina-coated np-Au film was

mounted onto the bottom surface of microfluidic platform over the fluid access window and sealed by applying epoxy along the perimeter of the chip. Three-electrode configuration was assembled through the microfluidic device holder. Fluorescein was loaded into the film by applying a positive voltage on the alumina-coated np-Au electrode while the microfluidic channel was infused with 10 mM fluorescein solution prepared in PBS. After one hour of loading under applied voltage, the microfluidic channel was rinsed with fresh PBS while maintaining the applied positive voltage to retain the fluorescein molecules inside the np-Au network. Finally, the loading capacity of fluorescein-loaded alumina-coated np-Au was determined when the fluorescein molecules were fully released. A negative voltage was applied on the fluorescein-loaded np-Au electrode to speed up the releasing process. Following the fluorescein release, the same alumina-coated np-Au film was loaded again following the same protocol stated above.

*Release measurement*: For fluorescein release under electrical voltage and open-circuit voltage, the fluorescein molecules migrated out of the np-Au films and dispersed into the flowing elution medium towards the observation region below the microscope objective, where a short time-lapse video (20 frames that lasted for 6 seconds) was recorded with an inverted fluorescence microscope. Each video sample was then uploaded to ImageJ[30] and the intensity of every frame inside the sample was extracted into a grey value with a timestamp. A calibration curve finally converted the intensity value to the fluorescein concentration. In the closed-loop controlled release experiment, LabVIEW program was used to continuously capture the time-varying fluorescence intensity. A live video of the microfluidic channel under fluorescence microscope was displayed and each real-time frame of the video was analyzed and extracted to determine the intensity from a user-defined region-of-interest in the channel.

**Supporting Information**
Supporting Information is available from the Wiley Online Library or from the author.

**Acknowledgements**

We gratefully acknowledge the support from National Science Foundation Awards (CBET-1512745 and CBET&DMR-1454426). We thank Dr. Monika Biener for preparing atomic layer deposition of alumina on np-Au samples and Dr. Ling Wang for assisting with electrochemistry experiments.

Received: ((will be filled in by the editorial staff))
Revised: ((will be filled in by the editorial staff))
Published online: ((will be filled in by the editorial staff))

References

[1] J. V. Natarajan, A. Darwitan, V. A. Barathi, M. Ang, H. M. Htoon, F. Boey, K. C. Tam, T. T. Wong, S. S. Venkatraman, *ACS Nano* **2014**, 8, 419.

[2] W. Eisenreich, B. Sommer, S. Hartter, W. H. Jost, *Parkinsons Dis* **2010**, 2010, 612619.

[3] S. Hua, E. Marks, J. J. Schneider, S. Keely, *Nanomedicine* **2015**, 11, 1117.

[4] G. M. Currie, J. M. Wheat, H. Kiat, *Open Cardiovasc Med J* **2011**, 5, 130.

[5] R. L. Nation, A. M. Evans, R. W. Milne, *Clin Pharmacokinet* **1990**, 18, 37.

[6] R. T. Timmer, J. M. Sands, *J Am Soc Nephrol* **1999**, 10, 666.

[7] a) H. C. Zisser, *Diabetes Ther* **2010**, 1, 10; b) P. Mage, B. Ferguson, D. Maliniak, K. Ploense, T. Kippin, H. Soh, *Nature Biomedical Engineering* **2017**, 1, 0070.

[8] a) E. Meng, T. Hoang, *Adv Drug Deliv Rev* **2012**, 64, 1628; b) A. Nisar, N. Afzulpurkar, B. Mahaisavariya, A. Tuantranont, *Sensors Actuators B: Chem.* **2008**, 130, 917.

[9] W. M. Pardridge, *NeuroRx* **2005**, 2, 3.

[10] Y. Fu, W. J. Kao, *Expert Opin Drug Deliv* **2010**, 7, 429.

[11] a) L. L. Lao, S. S. Venkatraman, N. A. Peppas, *Journal of Biomedical Materials Research Part A* **2009**, 90, 1054; b) M. J. Pereira, B. Ouyang, C. A. Sundback, N. Lang, I. Friehs, S. Mureli, I. Pomerantseva, J. McFadden, M. C. Mochel, O. Mwizerwa, P. Del Nido, D. Sarkar, P. T. Masiakos, R. Langer, L. S. Ferreira, J. M. Karp, *Adv Mater* **2013**, 25, 1209.

[12] A. Berenyi, M. Belluscio, D. Mao, G. Buzsaki, *Science* **2012**, 337, 735.

[13] a) M. Abidian, D. Kim, D. Martin, *Adv. Mater.* **2006**, 18, 405; b) A. Jonsson, S. Inal, I. Uguz, A. J. Williamson, L. Kergoat, J. Rivnay, D. Khodagholy, M. Berggren, C. Bernard, G. G. Malliaras, *Proceedings of the National Academy of Sciences* **2016**, 113, 9440.

[14] J. Erlebacher, M. J. Aziz, A. Karma, N. Dimitrov, K. Sieradzki, *Nature* **2001**, 410, 450.

[15] P. Daggumati, S. Appelt, Z. Matharu, M. Marco, E. Seker, *J. Am. Chem. Soc.* **2016**, 138, 7711.

[16] a) T. S. Dorofeeva, E. Seker, *Nanoscale* **2016**, 8, 19551; b) M. Hakamada, M. Mabuchi, *J Mater Res* **2009**, 24, 301; c) T. Siepenkoetter, U. Salaj-Kosla, X. Xiao, S. Belochapkine, E. Magner, *Electroanalysis* **2016**.

[17] a) O. Polat, E. Seker, *The Journal of Physical Chemistry C* **2016**, 120, 19189; b) T. Siepenkoetter, U. Salaj-Kosla, X. Xiao, P. Ó. Conghaile, M. Pita, R. Ludwig, E. Magner, *ChemPlusChem* **2017**, 82, 553; c) A. J. Alla, F. B. d'Andrea, J. K. Bhattarai, J. A. Cooper, Y. H. Tan, A. V. Demchenko, K. J. Stine, *J. Chromatogr.* **2015**, 1423, 19.

[18] a) C. A. R. Chapman, H. Chen, M. Stamou, J. Biener, M. M. Biener, P. J. Lein, E. Seker, *Acs Appl Mater Inter* **2015**, 7, 7093; b) E. Seker, Y. Berdichevsky, K. J. Staley, M. L. Yarmush, *Adv Healthc Mater* **2012**, 1, 172.

[19] C. A. R. Chapman, L. Wang, H. Chen, J. Garrison, P. J. Lein, E. Seker, *Adv. Funct. Mater.* **2017**, 27, 1604631.

[20] a) Z. Li, E. Seker, *Lab Chip* **2017**, 17, 3331; b) S. D. Gittard, B. E. Pierson, C. M. Ha, C. A. M. Wu, R. J. Narayan, D. B. Robinson, *Biotechnol J* **2010**, 5, 192; c) Y. Xue, J. Markmann, H. Duan, J. Weissmuller, P. Huber, *Nat Commun* **2014**, 5, 4237; d) G. M. Santos, F. Zhao, J. Zeng, W.-C. Shih, *Nanoscale* **2014**, 6, 5718.

[21] O. Kurtulus, P. Daggumati, E. Seker, *Nanoscale* **2014**, 6, 7062.

[22] O. Polat, E. Seker, *The Journal of Physical Chemistry C* **2015**, 119, 24812.

[23] a) X. Yan, X. Ge, S. Cui, *Nanoscale Res Lett* **2011**, 6, 313; b) Y. H. Tan, J. A. Davis, K. Fujikawa, N. V. Ganesh, A. V. Demchenko, K. J. Stine, *J Mater Chem* **2012**, 22, 6733.

[24] M. Biener, J. Biener, A. Wichmann, A. Wittstock, T. F. Baumann, M. B umer, A. Hamza, *Nano Lett.* **2011**, 11, 3085.

[25] J. J. Gulicovski, L. S. Cerovic, S. K. Milonjin, *Mater Manuf Process* **2008**, 23, 615.

[26] R. W. Sabnis, *Handbook of acid-base indicators*, CRC Press, Boca Raton **2008**.

[27] B. Ki Min, S. K. Kim, S. Jun Kim, S. Ho Kim, M. A. Kang, C. Y. Park, W. Song, S. Myung, J. Lim, K. S. An, *Sci Rep* **2015**, 5, 16001.

[28] a) M. Sedighizadeh, A. Rezazadeh, *Proc Wrld Acad Sci E* **2008**, 27, 257; b) C. W. Anderson, D. C. Hittle, A. D. Katz, R. M. Kretchmar, *Artif Intell Eng* **1997**, 11, 421.

[29] C. A. Chapman, N. Goshi, E. Seker, *Adv. Funct. Mater.* **2017**.

[30] J. Schindelin, I. Arganda-Carreras, E. Frise, V. Kaynig, M. Longair, T. Pietzsch, S. Preibisch, C. Rueden, S. Saalfeld, B. Schmid, J. Y. Tinevez, D. J. White, V. Hartenstein, K. Eliceiri, P. Tomancak, A. Cardona, *Nat Methods* **2012**, 9, 676.

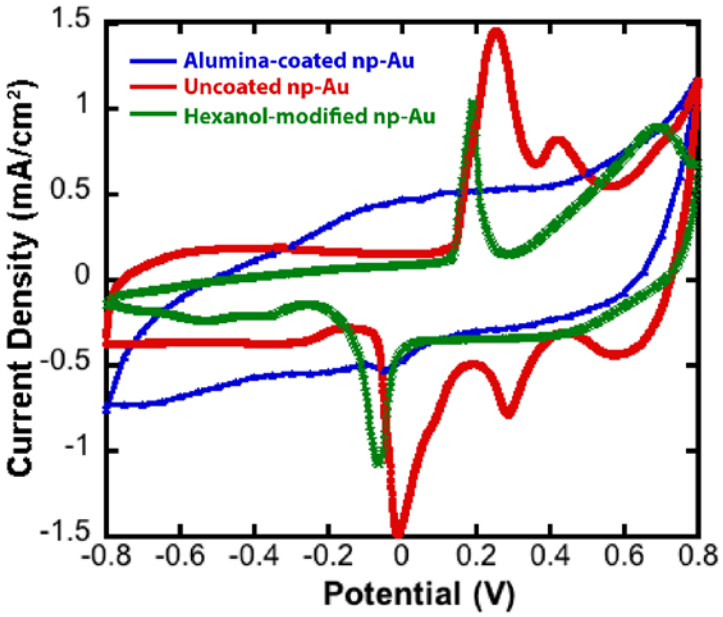


**Figure 1.** Cyclic voltammograms of uncoated np-Au, hexanol-modified np-Au, and alumina-coated np-Au. While the alumina-coated np-Au exhibited a purely capacitive voltammogram, the bare and hexanol-modified np-Au both led to undesirable faradaic reactions.

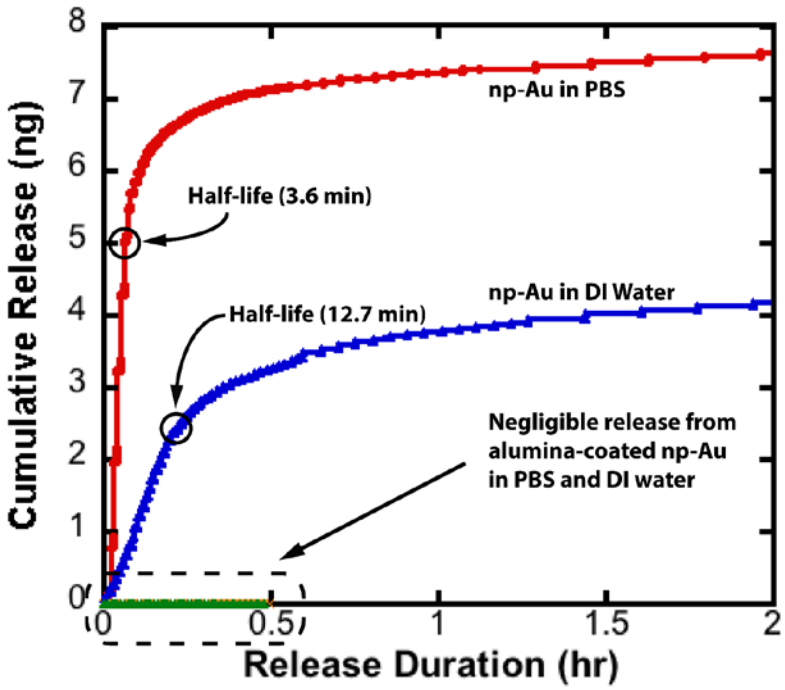


**Figure 2.** Cumulative release profiles from alumina-coated and uncoated np-Au in DI water and PBS. The region within dashed line box indicates the negligible release from alumina-coated np-Au in PBS and DI water. The half-life shown for the release of np-Au in PBS and DI water is based on the entire release duration of approximately ten hours (data for the entire release duration is shown in **Figure S1**).

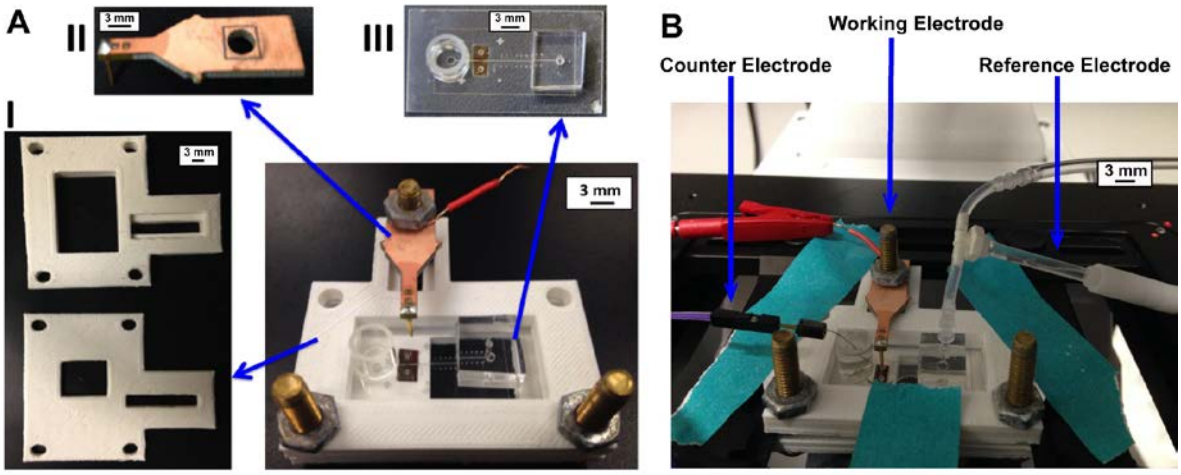


**Figure 3**. A) Release measurement setup with three components: I) 3D-printed microfluidic chip holder; II) laser-cut printed circuit board; III) microfluidic device. B) The three-electrode setup.

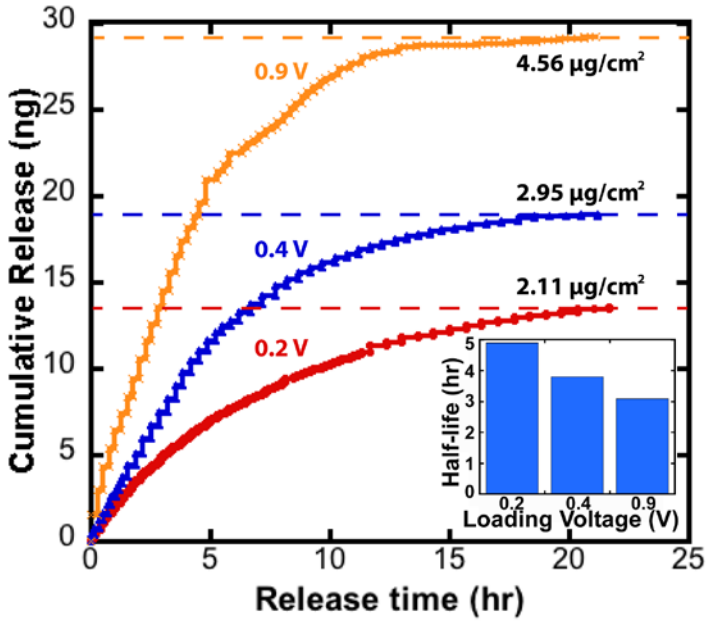


**Figure 4**. The cumulative release profiles for alumina-coated np-Au under different loading voltage (0.2 V, 0.4 V and 0.9 V) and same release voltage (-0.5 V). Inset shows the half-life of the release from three loading voltages.

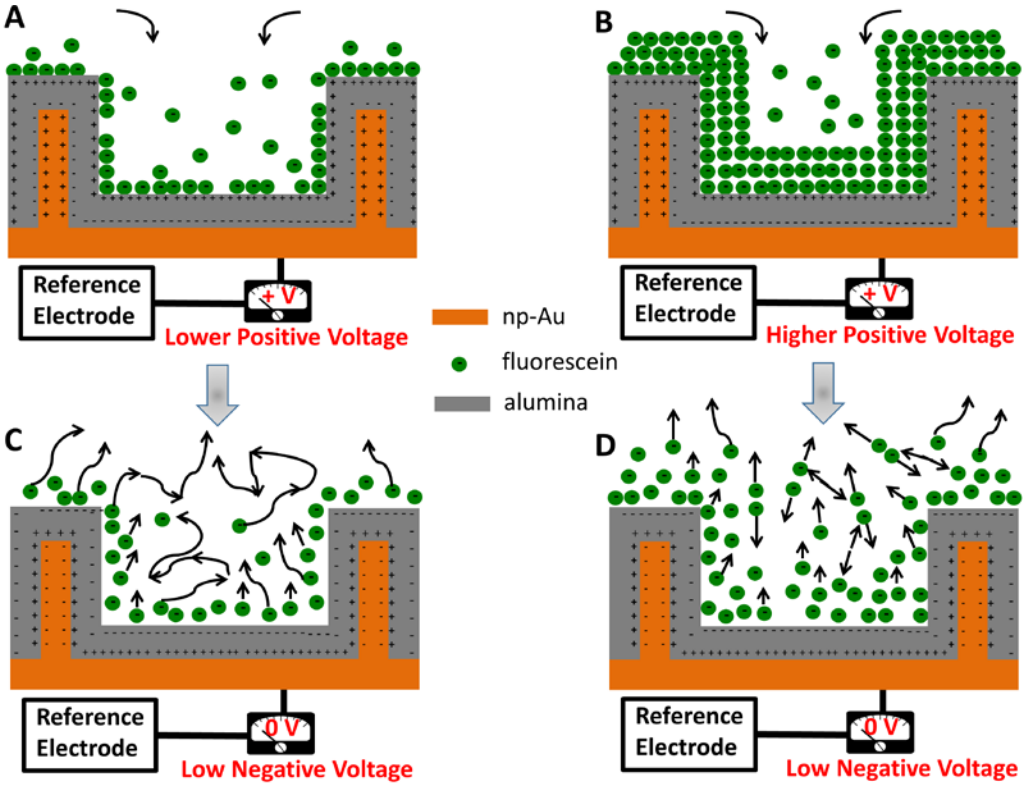


**Figure 5**. Schematic illustration of loading and releasing processes. Under positive loading voltage, A) negatively-charged fluorescein molecules are attracted and electrically screened on the alumina surface. B) With higher applied voltages, more fluorescein molecules are attracted to the surface to conserve the charge balance, leading to the thicker multi-layer stacking on the alumina surface. When the voltage is removed, D) the electrostatic repulsion accelerates the fluorescein dispersion by increasing the mobility of the particles compared to C) the dispersion of neutral particles (which is driven by random Brownian motion - diffusion) that are loaded under open circuit voltage.

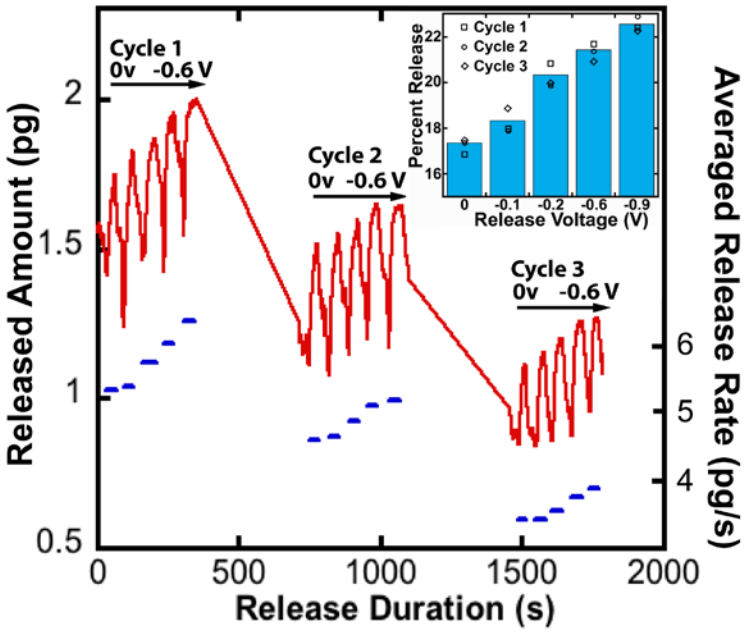


**Figure 6**. The instantaneous release profile (red) of fluorescein under negative voltage during three repeated cycles. In each cycle, different release voltages (0 V, -0.1 V, -0.2 V, -0.4 V and -0.6 V) were applied sequentially for the same duration (30 s) and a positive voltage of +1 V was applied in between. The average release rates during each release voltages are shown as blue dashes corresponding to the cycles above them. Inset shows the percent amount of fluorescein released under each voltage with respect to the total released amount in each cycle. The blue column indicates the averaged relative fluorescein release across the three cycles.

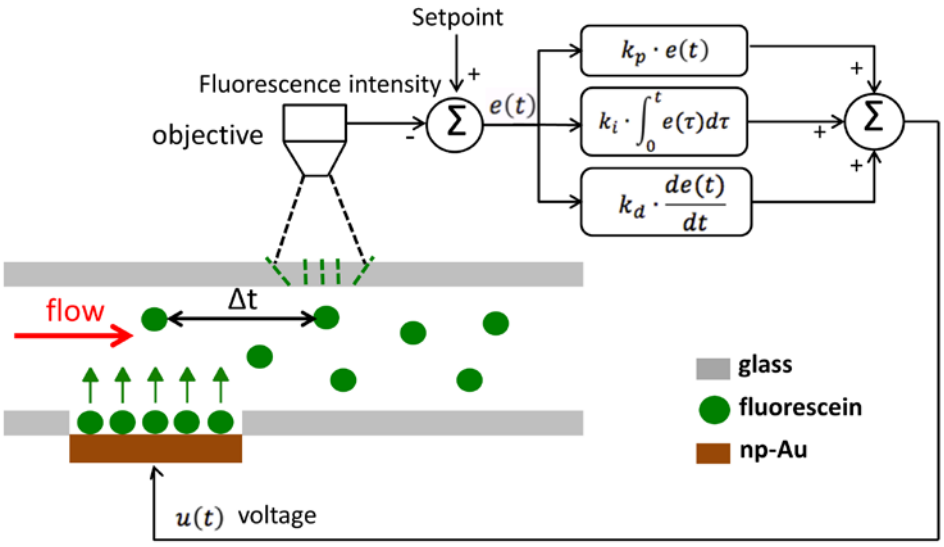


**Figure 7**. Schematic representation of the closed-loop controlled molecular release system. Serving as the indicator of fluorescein concentration, the fluorescence intensity is acquired by the fluorescence microscope and compared with the intended release amount (set-point). The difference e(*t*) is fed to a proportional-integral-derivative (PID) controller, which computes the output voltage u(*t*). The voltage is subsequently applied on the np-Au electrode for triggering or suppressing the release. The released fluorescein travels down the microfluidic channel through the microscope observation area for fluorescence quantification. The convective transport time from np-Au to below the objective constitutes the response delay, *Δt*, of the controller.

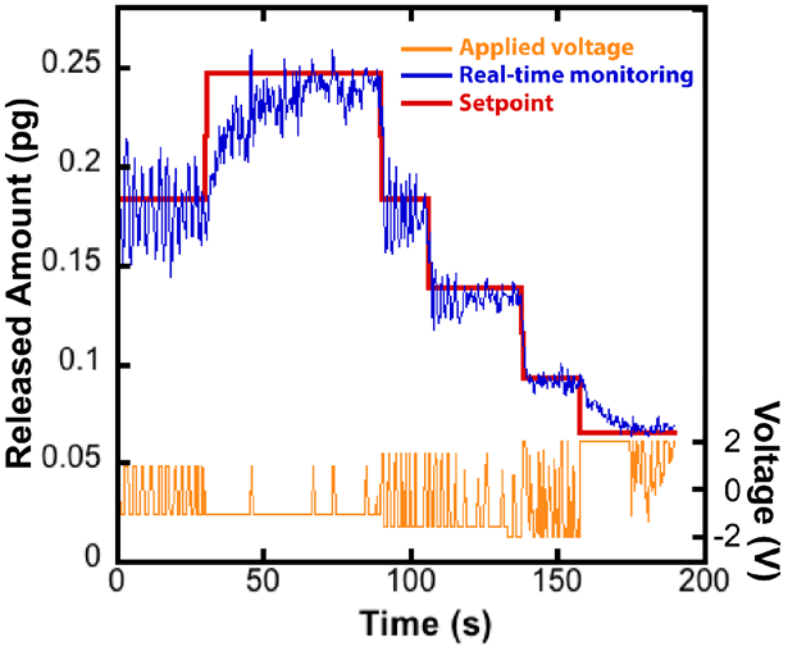


**Figure 8**. The instantaneous release profile of fluorescein (blue) under closed-loop control via applied voltage (orange) to achieve the arbitrary release profile defined by the staircase-like setpoint (red).

**Alumina-coated nanoporous gold (np-Au) electrodes allow for voltage-gated closed-loop control of small-molecule release.** Via leveraging electrical conductivity, microfabrication compatibility, and high effective surface area of np-Au, arbitrary waveforms of release dose are attained, paving the way to the effective management of disorders with time-varying therapeutic windows.

**Keywords:** gold, porous materials, functional coatings, drug delivery

Zidong Li, Ozge Polat, Erkin Seker*

**Voltage-Gated Closed-Loop Control of Small-Molecule Release from Alumina-Coated Nanoporous Gold Thin Film Electrodes**